Pulse modulated TIG welding to influence corrosion resistance on UNS S32205

Julia Wichmann*, Stefan Ulrich*

*** Günter-Köhler-Institut für Fügetechnik und Werkstoffprüfung, Jena, Germany**

This paper presents the influence of the pulse modulation in TIG-welding on the pitting corrosion resistance. The reason for pitting corrosion is an inhomogeneous distribution of austenite across the cross-section of the welds of thin-walled structures produced by tungsten inert gas welding (TIG) without filler metal. This leads to increased susceptibility to corrosion. The question arises as to how the potential can be better exploited by using pulse-modulated TIG processes. The corrosion tests were carried out in a modified test setup following ASTM G150. To accelerate the aging process the samples were tested in a 6 % ferric chloride solution containing 20 % HCl. These tests are intended to contribute to answering the question.
In the investigations, the basis was a non-pulsed TIG process, on which the pulse modulation of the welding current was based. Initial investigations showed a positive influence on the phase ratio with regard to austenite and a reduction in grain size through the use of medium-frequency pulsing of the welding current. Proceeding with those results, a high-frequency pulsing was superimposed in the high and base current phases as well as in the flank sections to assess the effects on the microstructure and corrosion resistance. On the basis of the prepared welds, the microstructure was characterized in addition to determining the corrosion resistance. Correlation with the pulse parameters allowed a relation to be established between the microstructure in the weld metal and the heat-affected zone with the formation of pitting and its location.

KEYWORDS: PULSE MODULATED TIG WELDING-DUPLEX STAINLESS STEEL-PITTING CORROSION RESISTANCE-AUSTENITE CONTENT

INTRODUCTION

The substitution of austenitic stainless steels with duplex stainless steels is steadily increasing. However, the growing market demands a reliable and economical joining process. In addition, the last few years have shown an unsteady increase in raw material prices, especially for the alloying element nickel, which is used in high quantities in the established austenitic grades. In order to remain marketable in a highly competitive economy, it is essential to have relatively stable and thus calculable costs for raw materials. Duplex stainless steels are used in applications where they benefit in terms of corrosion resistance and/or strength compared to other stainless steels.
Usually austenitic stainless steels can be welded without filler metal, while welding duplex steels requires filler metal. For example, the “German Welding Society” (DVS), NORSOK and/or the stainless steel information office recommend using filler metal when welding duplex stainless steels in order to influence the properties of the weld metal positively, mainly with regard to corrosion resistance and notched bar impact strength [1-3]. The aim of the addition is to counteract the segregation and evaporation of important alloying elements, thus reducing the risk of nitride precipitation and forcing the formation of austenite.

Apart from the use of filler metal, the phase ratio of austenite to ferrite depends largely on the energy input and its type during welding. In TIG welding, this determines the cooling rate and ultimately the austenite content, since the transformation of ferrite into austenite is diffusion-controlled. Depending on the material thickness, the recommended energy per unit length should be between 2 to 35 kJ/cm for arc processes [4-7]. These values usually only serve as guidelines, since they often do not consider the efficiency of the respective process. Herzmann et al. and Karlsson recommend energy per unit length between 3-25 kJ/cm specifically for the S32205. In the industrial sector, the line energy is usually between 5 and 25 kJ/cm, but this assumes a thermal efficiency of one [6, 8]. In this range, austenite contents of ≈50 % can be achieved, but a balanced phase ratio alone does not contribute to corrosion resistance. It was shown, that in TIG welding with pure argon, the energy input is a decisive factor. This is due to the fact that corrosion is facilitated by both a line energy close to the process boundary for through-welding (high cooling rate) and for melt pool breakdown (high nitrogen loss). Both mechanisms result in high ferrite content. In several investigations on different duplex grades, line energies of 7-9 kJ/cm were the most suitable to reduce the susceptibility to pitting corrosion. [5,

7, 8] In addition, Westin et al. and Pettersson et al. showed that even welds with high ferrite content could still exhibit high pitting resistance when working with gas mixtures [9-10]. Besides an unbalanced phase ratio, the risk of pitting corrosion increases with the formation of chromium nitrides in the ferrite matrix. Chromium nitrides lead to chromium depletion both at the grain boundaries and within the ferrite grain [11-13]. Nitrogen loss/chromium depletion contributes mainly to a local decrease in corrosion resistance. [6, 9-12, 14]

In order to utilize the advantages of TIG welding for duplex stainless steels, it would be desirable to develop a process requiring no use of filler metal or subsequent heat treatment. Beyond the pure cost savings, the reduced complexity for the automatisation of the welding process would in turn increase its attractiveness.

Since the 2000s, results on pulsed TIG welding without the addition of filler metal of duplex stainless steels have been steadily published. In these, a square-wave pulse was used. Wang et al. investigated the influence of pulsing at a frequency of 500 Hz on the microstructure of S32205. They were able to show that the higher cooling rate during pulsing favoured intragranular austenite (γ_2) nucleation and growth. The austenite content increased from 11 % to 19 % which can be attributed to grain refinement. [15] Also, Palmer et al. also analysed the microstructure formation in the heat affected zone as well as the fusion zone of S32205 during plussed TIG welding and observed similar behaviour at f=300 Hz [16]. Coarser ferrite grains mean lower grain boundary density which in turn retards or inhibits austenite growth at grain boundaries during cooling. Wang as well as Palmer focused their investigations on austenite formation and mechanical properties. Regarding improvements in corrosion resistance, results by Yousefieh et al. show how crucial the combination of the high current and base current phases is for the corrosion resistance of the welds. At a difference of 60 A between the two current phases, the resistance to corrosion and the degree of grain refinement were the highest. From the ANOVA analysis, there was an effect of ≈92 % on the corrosion behaviour. Duty cycle and pulse frequency tended to play a minor role. As a conclusion, corrosion was a function of high current, base current phase as well as duty cycle. [13, 17] However, it should be considered that the selected frequencies were in the range of thermal pulsing (0,5-10 Hz) and not in the range of metallurgical pulsing (20-200 Hz) and high frequency pulsing (2-8 kHz).

Schellhase already described possibilities for metallurgical influencing and focusing of the arc, through the application of superimposed high-frequency pulses in TIG welding [18]. Further investigations by Dzelnitzki, Qi et al, Yang, M. et al and Zhou, Y. et al showed that in the frequency range of the metallurgical pulse, dendritic fragmentation is achieved by the pulsating molten pool. These melt pool dynamics are caused by the pulsating arc pressure. The pulsating arc itself causes the constriction of the plasma. This has a direct effect on the convection of the molten pool and increases its dynamic. In the higher frequency range, the arc is constricted, resulting in a higher energy density and thus promoting constitutional supercooling. In general, pulsed TIG welding is mainly suitable for thin-walled structures [19-22]. Based on these investigations, the following assumptions were concluded:

- Modulating the high-current phase (see **Figure 1**b) causes an impediment to dendrite growth.
- Pulse modulation of the base current phase, see **Figure 1**c, dynamically excites the weld pool, primarily in the solidification phase, due to the variable current.
- Pulse modulation of the current lowering phase (see **Figure 1**d) affects the weld pool as a "metallurgical oscillation" during the entire transition from melting to incipient solidification.

The continuous publication on superimposed pulse welding (or pulse modulation) further proves the topicality of this process as well as the existence of gaps in knowledge in this respect [23-25]. An approach and potential for pulsing in different phases is presented by Wang et al. using Al alloys as an example [26]. Pulsing is performed in both the high and base current phases.

In summary, DC pulsing in TIG welding has been considered in a large number of publications. The emphasis in older publications was mostly on frequencies <10 Hz. This is due to the limited capabilities of older power sources. Newer power sources offer the possibility to realize much higher pulse frequencies, up to 80 kHz. This is reflected in the publications. In both cases, the square-wave pulse form was and is currently essentially used. The investigations mainly focused on the mechanical-technological characteristics of the joint. The knowledge of what effect the modulation of the pulsed current has on the corrosion and metallurgical properties

during welding in the area of duplex steels is very sparse.

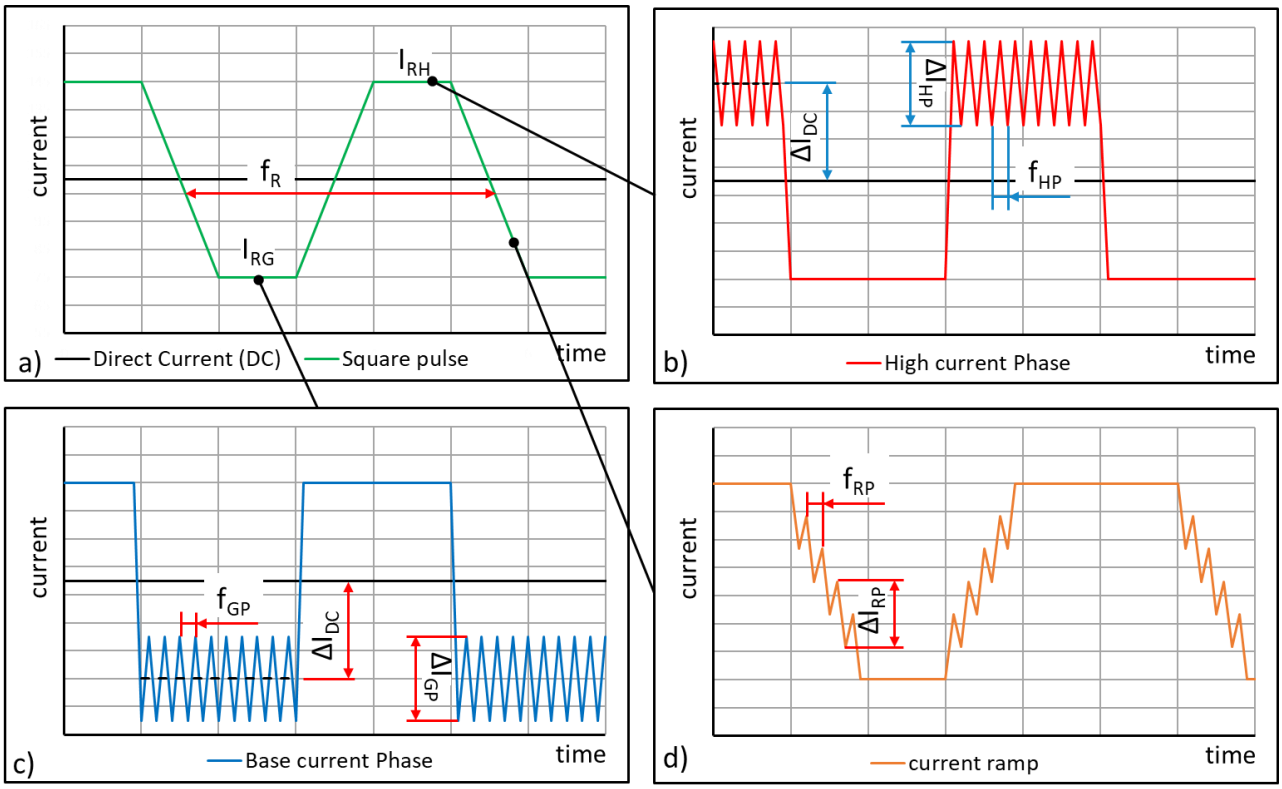

Figure 1: Current waveform DC (a) and square pulse (a), modulation high current phase (b), modulation base current phase (c), modulation current ramp (d)

Experimental

Material

The tested material was cold rolled X2CrNiMoN22-5-3 with a sheet thickness of d=2,0 mm and the chemical composition given in Table 1. This material is comparatively inexpensive to purchase on the market in a constant grade and is the most widely used alloy in the duplex steel sector in the industrial environment. More details on the material and TIG-process can be found in [1, 4, 18, 27].

Table 1: chemical composition from X2CrNiMoN22-5-3

	C [wt%]	Si [wt%]	Mn [wt%]	P [wt%]	S [wt%]	Cr [wt%]
DIN EN 10088-3	≤0,030	≤1,00	≤2,00	≤ 0,035	≤ 0,015	21,00- 23,00
tested	0,028	0,35	1,39	0,023	0,002	22,02
	Mo [wt%]	**Ni [wt%]**	**N [wt%]**	**Cu [wt%]**	**Nb [wt%]**	**Co[wt%]**
DIN EN 10088-3	2,50- 3,50	4,50- 6,50	0,10-0,22	-	-	-
tested	3,47	5,84	0,10	-	-	-

Welding

A JWT-R welding tractor (Jäckle) was coupled with a TIG torch for the investigations. To enable free modulation of the pulses, a modified welding current source from Rehm InvertigPRO Digital was used. Coupling with a Rigol DG1022Z arbitrary function generator, which is controlled via a laptop, free programming of the pulses was possible, see Figure 2.

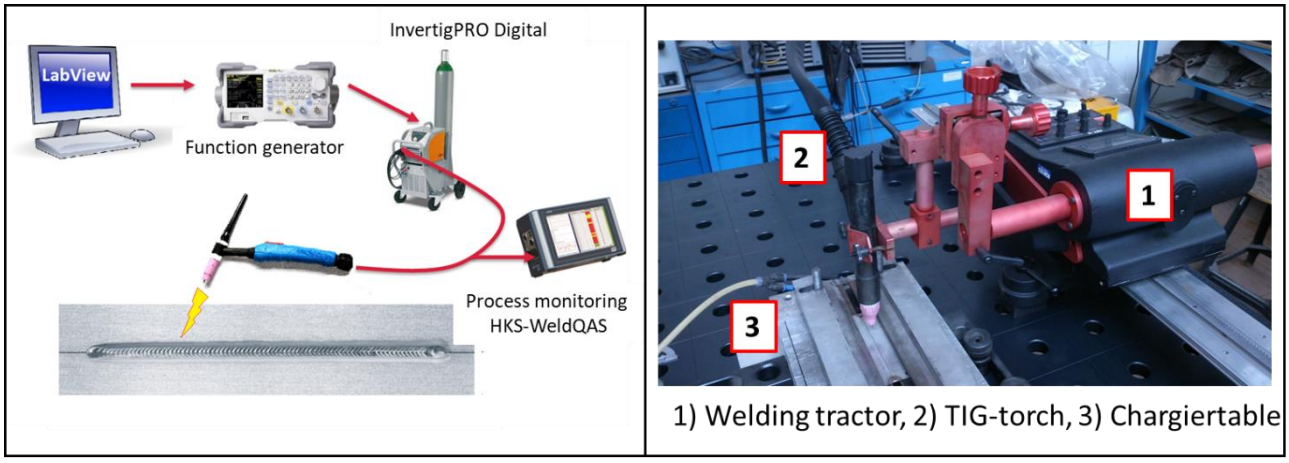

Figure 2: left-schematic experimental setup, right-Test setup

The welding tractor controls the welding speed so that the feed rate results from the relative movement between the stationary specimen plate and the torch. To form the root, argon 4.6.gas was used at 18 l/min as well as shielding gas with a flow rate of 10 l/min. A WGLA-15 lanthanum tungsten electrode was used with a diameter of 1,6 mm, perpendicularly positioned to the specimen with a working distance of 3 mm. The seam was listed as an I-seam in the butt joint. As a foundation for all subsequent experiments the welding current I_{DC}=93 A and welding speed 18 cm/min, resulting in an energy per unit length of 3,53 kJ/cm was used. with I = current [A], u= voltage [V], T=period [s], v= welding velocity [cm/min].

Table 2 lists the varied process parameters with their respective values. By forming an array, the experimental design is carried out with the aid of the Optislang software. The parameter combinations were chosen to correspond to the energy per unit length of the previously mentioned DC welding process. The energy varied between 3,34 kJ/cm and 3,70 kJ/cm. With the help of the measurement system Weld QAS the current vs. voltage signal was obtained and the line energy per unit could be calculated with formula 1:

$$E_S = \frac{P}{v} = \frac{1}{v} \cdot \frac{1}{T} \int_0^t (i(t) \times u(t))\, dt \qquad \text{Formula 1}$$

with I = current [A], u= voltage [V], T=period [s], v= welding velocity [cm/min].

Table 2: Parameter for pulse modulation

ΔI_{GP} [A]	ΔI_{HP} [A]	ΔI_{RP} [A]	ΔI_{DC} [A]	f_R [Hz]	f_{GP} [kHz]	f_{HP} [kHz]	f_{RP} [kHz]
10; 40	10; 40	10; 40	8; 17; 23; 33; 37	100; 200	1; 8; 15	1; 8; 15	2; 5; 8

Material Testing

The cross sections were cut and embedded, subsequently ground and polished using standard automated preparation techniques. Color etching using the immersion method with Beraha II (60 ml H_2O + 40 ml HCl + 1 g $K_2S_2O_5$) was used to prepare the transverse sections of each experiment. The average ferrite content in the weld was determined by optical image analysis using ImageJ software on 20 sections of the weld. With the help of a self-written macro in ImageJ, which tremendously sped up the image processing, the cross sections were analysed using a grayscale-threshold method with a subsequent particle analysation provided by the ImageJ software to determine the austenite phase fraction and the size of said phase regions. For the error analysis of this method a round rabbit test with 5 participants was carried out.

In preparation for the corrosion tests, discs of 15 mm diameter were cut from the welds and ground (#320, #600 and #1200 SiC) to remove welding oxides and seam irregularities. Finally, the specimen was polished by electrolytic polishing (40 V polishing voltage, 12 s duration, A2 polishing electrolyte by *STRUERS*). By reducing the influence of oxide layers, possible weld splatters and seam irregularities the determining influence on the corrosion remains the microstructure of the weld and thus the critical pitting temperature (CPT) can be increased [10, 28]. Among other things, this is attributed to nitrides or sigma phase. In addition, it could lead to a local dissolution of ferrite grains, which have a lower pitting corrosion resistance than austenite [28-29]. In order to rebuild the oxide layer evenly on the sample and thus to re-establish its protective character against pitting corrosion, the samples were passivated in 60°C warm distilled water for 1h before the corrosion test.

The corrosion tests were performed with a modified procedure, see Table 3. For faster aging, the more aggressive iron(III)chloride was used. Before the potential scan started, the open circuit potential (OCP) was determined at the starting temperature for 10 minutes. Because of possible metastable corrosion at current densities of 100µA/cm² and higher the CPT was determined by a regression analysis using the corrosion current vs. temperature plot. Among others, Johansson et al. point out this risk in their studies [30]. Since corrosion is a stochastic process, 4 samples were tested per parameter setup. In addition, the specimens were visually/microscopically examined in which area of the weld the pitting corrosion occurred. Specimens showing crevice corrosion were not included in the evaluation.

Table 3: Comparison of test methods

	ASTM G150		**ASTM G48 Method E**
Electrolyte	1 mol NaCl	6%ig FeCl +20 %ig HCl	6%ig FeCl +37 %ig HCl
Start temperature	0°C	10°C	0°C
Temperature rise	0,017±0,005 K/s	0,020±0,0012 K/s	1 K increase per test
Temperature stability	±0,4 K	±0,05 K	±0,5 K
invested potential	0,700 V_{SHE}	0,3≤V_{SHE}≤0,4	-
Sample surface	reproducible	polished	pickled
CPT	60 s long at 100 µA/cm²	Regressions analyse	$Ø_{Pitting}$ ≥ 25 µm
Test area	min. 1 cm²	1,0 cm²	min. 20 cm²

Results

Austenite content

Figure 3 shows how the pulse modulation of the base current phase at a pulse frequency of f_R=100 Hz affects the austenite formation. For the entire series of experiments, the energy per unit length was between 3,34 ≤ E_{St} ≤ 3,39 kJ/cm. The differences result from the fluctuations in the current and voltage values. A trend in regards to higher austenite content at lower modulation frequencies f_{GP} is clearly recognisable. The austenite content in the weld metal increases from 24,8 %(DC) to up to 27,3 %, with a mean standard deviation for the austenite content of ≈±1,0 %. In addition, austenite formation seems to be favoured by a combination of small amplitude current (ΔI_{GP}=10 A) and higher differential current (ΔI_{DC}). The selected amplitude frequency f_{GP} has minimal influence. If, on the other hand, the pulse frequency f_R is increased to 200 Hz, the influence of the amplitude frequency f_{GP} increases, as a linear dependence on the austenite content is shown. The austenite content tends to decrease with increasing frequencies f_R and f_{GP} up to 21,4 %.

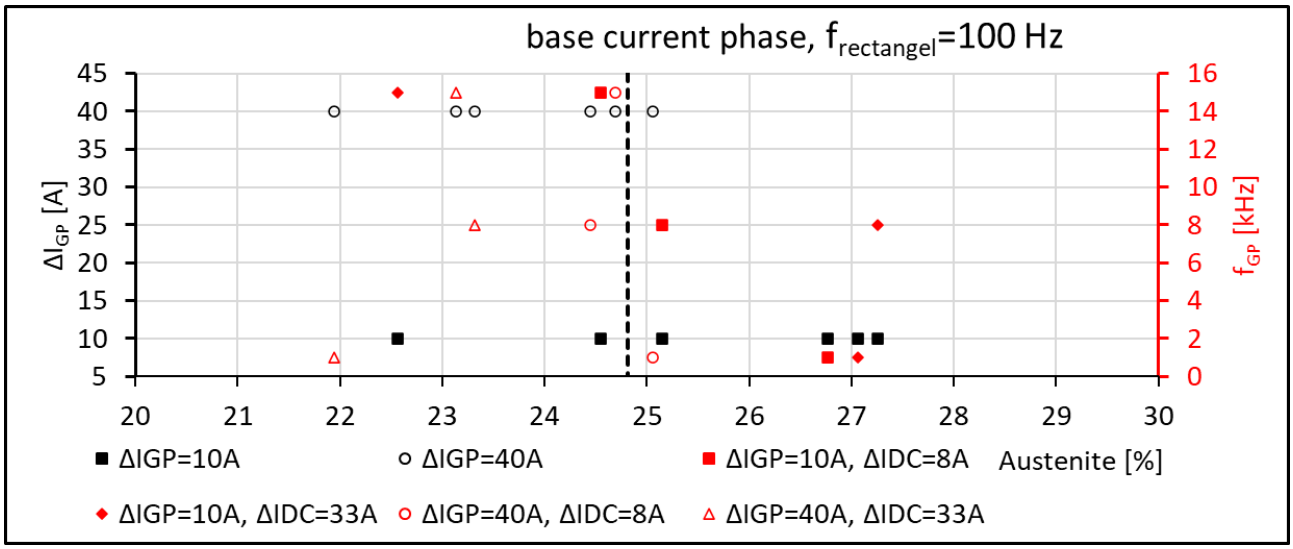

Figure 3: Resulting austenite content with modulation of the base current phase by f_R=100 Hz (dashed black line DC)

In the high current phase, however, an inverted trend emerges. At lower base frequencies f_R=100 Hz, the austenite content was lowered compared to the DC process. The highest austenite content of 24,7 % resulted

from the parameter setup with high frequency modulation (f_{HP}=15 kHz) of the amplitude current at ΔI_{HP}=10 A and low differential currents (ΔI_{DC}). **Figure 4** shows that at f_R=200 Hz an improvement could only be achieved with one parameter set. At high differential and amplitude current, an austenite content of up to 27,3 % can be achieved.

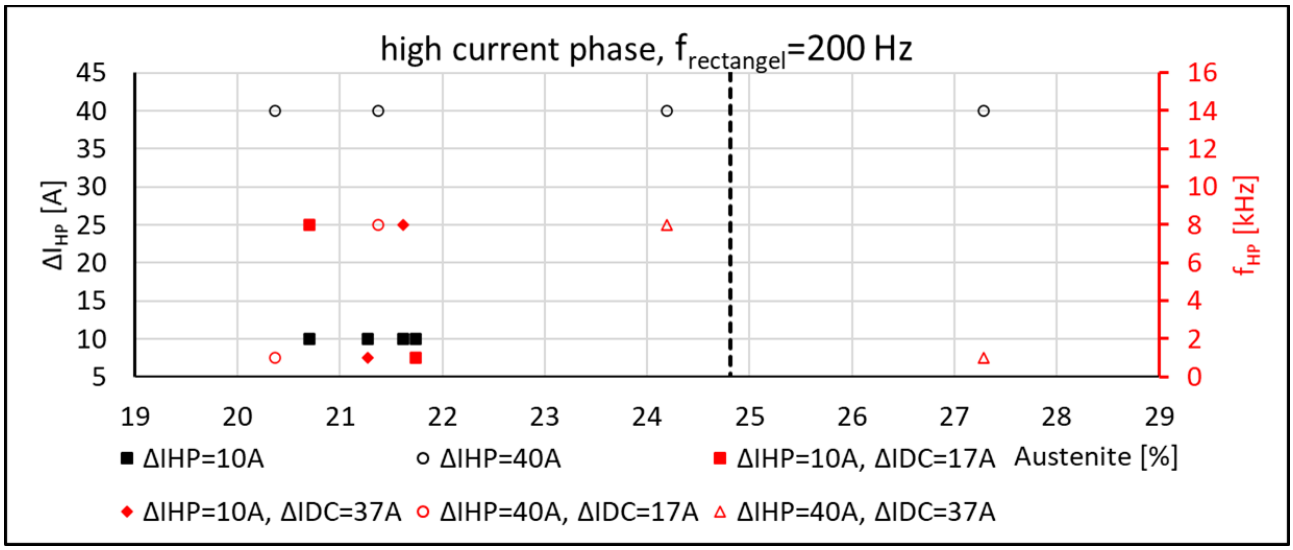

Figure 4: Resulting austenite content with modulation of the high current phase by f_R=200 Hz (dashed black line DC processes)

The most effective way to increase the austenite content is to modulate the flank current. At a ratio of falling to rising edge of 2, the austenite content increased from 24,8 % (DC) to 28,9 % when the frequency was f_R=200 Hz and f_{RP}=5 kHz at a modulated amplitude current of ΔI_{RP}=10 A. Although there was a decrease in the energy per unit length from 3,53 kJ/cm at DC to 3,48 kJ/cm. This may lead to a higher ferritic weld metal as austenite formation is a time dependent process (high cooling rates inhibit austenite formation). However, Wang et al. assumed that in pulsed processes, at high cooling rates, there is a higher driving energy for the nucleation of austenite due to greater undercooling [15]. In addition, it was shown that for different parameter setups almost the same result was obtained with regard to the austenite content. These are circled in green in **Figure 5**. For a constant modulated amplitude current of ΔI_{RP}=10 A, the variation of the base frequency f_R at f_{RP}=5 kHz does not seem to have a significant influence on the resulting austenite content. However, the analysis of the microstructure and the distribution of austenite and ferrite phase fractions and their average size shows dependencies, see section Microstructure.

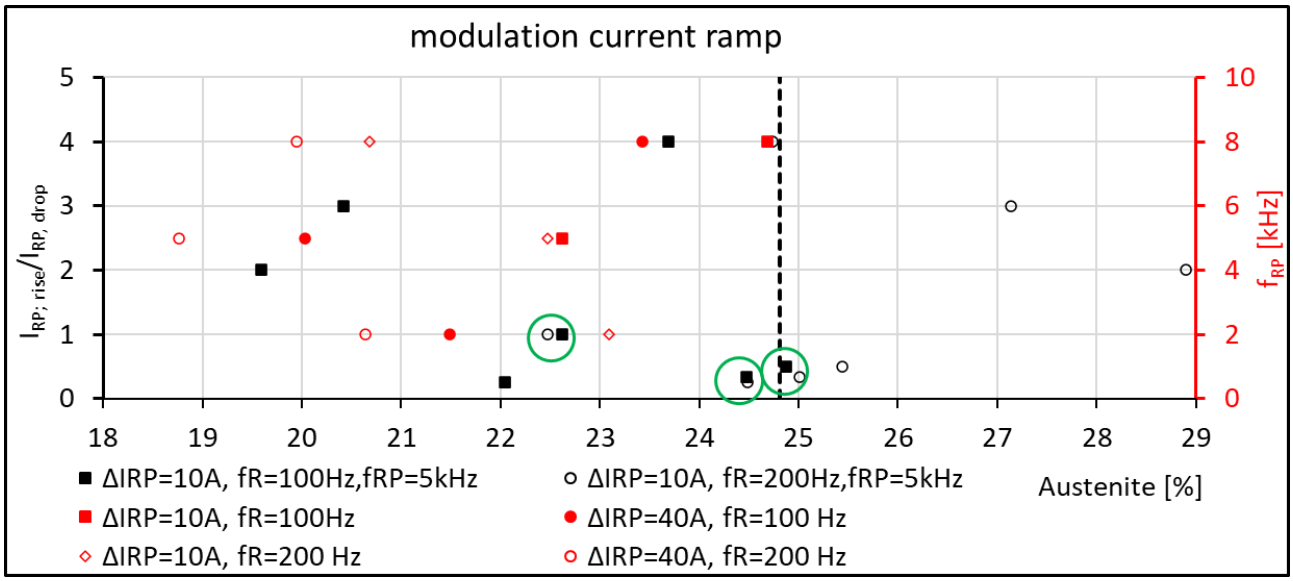

Figure 5: Resulting austenite content with modulation current ramp (dashed black line DC processes)

Microstructure

The analysis of the micrographs of the modulated base current phase shows a predominantly intergranular austenite formation along the ferrite grain boundaries. In addition, with increasing amplitude current, more Widmannstätten austenite was formed and the intragranular precipitated austenite exhibited a predominantly elongated morphology. When examining the microstructure, there were no signs of sigma phase formation. At frequencies of f_R=200 Hz in combination with a high differential current (ΔI_{DC}) to the DC process, nitrides could be detected.

If the value of the phase regions (averaged value from min. and max. expansion) of the austenite was in the order of magnitude of the pure DC process, the austenite content was 1,3-3.5 % lower than the austenite content of the DC process. For ferrite, this simultaneously led to an increase in phase region size from ≈1900 µm (DC) to ≈2600 µm to 4500 µm, which in turn led to coarse grain formation of the ferrite. In the case of austenite, this simultaneously led to an increase in the individual surfaces. There tended to be no dependencies with regard to the process parameters.

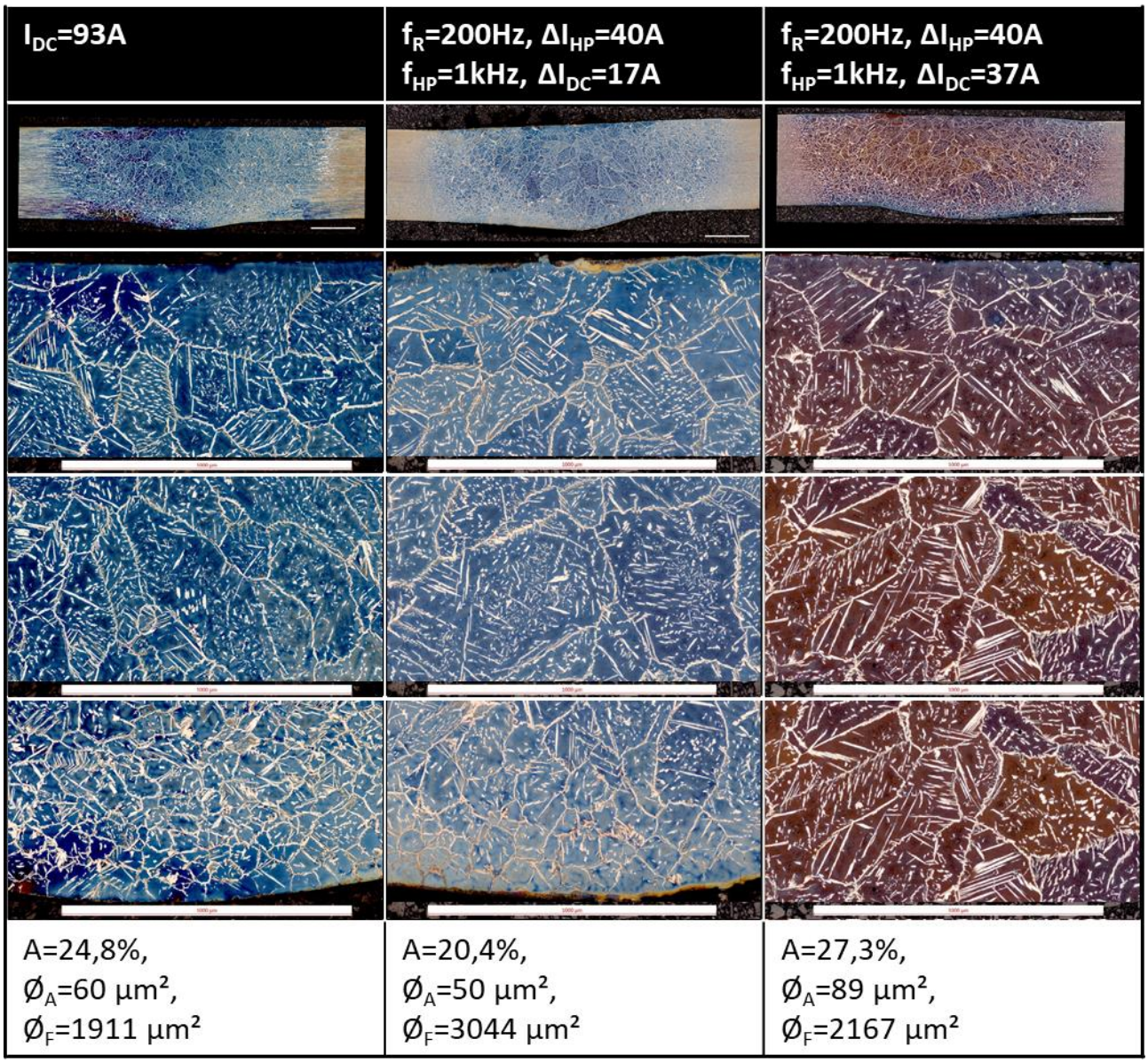

Figure 6: First row: Overview images, second row: Top layer, third row: fusione zone, fourth row: root layer, from left to right: pure DC process, pulse modulation of the high current phase with varying differential currents ΔI_{DC}

If the austenite content was significantly higher than in the DC process, the distribution of the austenite and ferrite phase regions was different. The extent and number of ferrite regions were more in line with that of the

DC process. In comparison, the austenitic zones grew from $Ø_{DC}$=60 µm to $Ø_{GP}$=85 µm, although the energy per unit length was 0,15 kJ/cm lower, with the same phase ratio as in the DC process.

The microstructural analysis of the test series of the modulated high current phase proves that the formation of Widmannstätten austenite was increasingly suppressed. However, the risk of nitrides forming increased. The form in which austenite formed was strongly dependent on the level of the differential current ΔI_{DC} to the. Comparing the parameter ΔI_{DC}=17 A with ΔI_{DC}=37 A, the expansion of the spattered intragranular austenite increased. In addition, grain refinement is assumed to occur when the frequency f_R is increased from 100 Hz to 200 Hz, as indicated by the average size of the ferrite phase regions in **Figure 6**. A numerical analysis showed that the increasing size of the austenitic zones is linearly related to the increasing austenite content. With a coefficient of determination R^2=0,91 at f_R=100 Hz and R^2=0,98 at f_R=200 Hz, this dependence can also be described as significant. With regard to the corrosion resistance, the austenite depletion in the top and root layer area could have a negative effect.

When evaluating the pulse modulation of the flanks, it was noticeable that at a ratio of flank rise to flank fall of less than 1, nitrides formed in the centre of the weld. With decreasing base frequency f_R and decreasing austenite content, nitride formation increased. With regard to the average phase fraction sizes of ferrite and austenite, a different behaviour than in the base current or high current phase modulation can be seen. If the resulted microstructure was characterised by very small ferrite phase regions of high number, the individual austenite zones grew in size. This is in contrast to the other two modulation phases. In those, the austenite and ferrite grew simultaneously. There was also a tendency for a linear dependence of the size of the austenite on the austenite content with R^2=0,85 at f_R=100 Hz and R^2=0,88 at f_R=200 Hz. While the austenite content was almost the same for different parameter setups, the number of austenite zones, at $I_{RP;\,rise}/I_{RP,\,drop} \neq 1$, increased with increasing frequency f_R. This increase was mainly reflected in finely precipitated spattered intragranular austenite. Due to the growing ferrite phase regions, the austenite precipitated at ferrite grain boundaries decreased at the same time. Over the entire test series, hardly any Widmanstätten austenite was formed in the samples prepared with a flank pulse modulation.

Pitting corrosion

In the evaluation of the corrosion tests, the critical pitting temperature for high current phase modulation samples with a base frequency of f_R=200 Hz was above that of the pure DC process (cpt=42,2°C±0,7 K),. The highest resistance to corrosion (cpt=45,5°C±1,5 K) was achieved at a modulation frequency of f_{HP}=8 kHz with ΔI_{HP}=10 A and high differential current ΔI_{DC}=37 A. With decreasing line energy from 3,41 kJ/cm to 3,34 kJ/cm, the scattering between the individual parameter setups decreased and the critical pitting temperature increased, independent of the modulation frequency. A clear dependence of the microstructure on the place of origin of the pitting corrosion was not recognisable.

The main component of the present work was to investigate the influence of the pulse modulation in the three phases basic and high current phase as well as the flank on the corrosion resistance. However, the optimisation of the welding parameters was beyond the scope of this work.

If the top layer had a pronounced ferrite seam, increased corrosion attack was observed in this area. This can be attributed to the loss of nitrogen, among other things, since pure argon was used for welding. This fringe was more pronounced at high line energies than at lower ones. Brytan et al. assumed that the associated higher susceptibility to corrosion is related to increased nitrogen loss at higher line energies [5]. Similar behaviour was also reported by Westin et al. and Pettersson et al [9, 10].

The chromium nitrides formed in some samples did not simultaneously lead to a reduction in corrosion resistance. The authors assume, that the corrosion resistance was reduced when the chromium nitrides were present in the edge areas (top/root layers). For further investigations, this means that there is no "automatic" increase in susceptibility to pitting corrosion when chromium nitrides are bonded. This is in line with the findings of the investigations by Lilijas et al [31].

It is often required that the ferrite content of the weld metal should be in the range of 35 – 65 % [1-3], although the phase fraction itself is not a property. Despite differences in the ferrite content and the predominantly too high ferrite content, the results of the corrosion measurement have shown that a high resistance is achievable,

see **Figure 7**. In **Figure 7**, the austenite content is compared with the critical pitting temperature for the modulated high current phase. Using Formula 2 the theoretical cpt of the base material can be calculated with the chemical composition from **Table 1**.

$$cpt\ (^{\circ}\ C) = \left(2.5\ \times \%\ Cr\right) + (7.6 \times \%Mo) + (31.9 \times \%N) - 41 \qquad \text{Formula 2}$$

The calculated cpt for the base metal is shown with a dashed line and the measured cpt=48,3°C±0,4 K for the base material is shown in blue. Even the austenite content of less than 25 % mentioned by Hsieh as unacceptable did not have an exclusively negative effect on the corrosion resistance [32]. It is noticeable that the standard deviation decreases with increasing critical pitting temperature. A clear assignment of the area of the weld where pitting corrosion preferentially occurred was not detectable. Regardless of the modulation frequency and whether f_R=100 Hz or f_R=200 Hz was used, in contrast to the pure DC process, the point of origin in HAZ and FZ was arbitrary and did not follow any systematic.

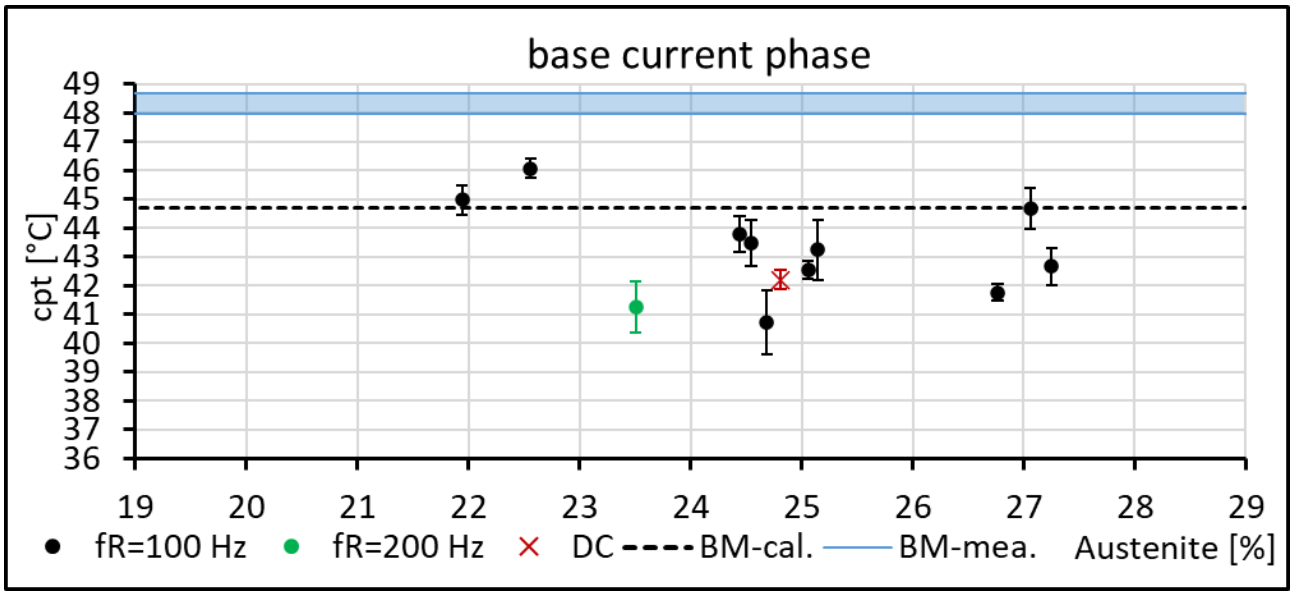

Figure 7: Influence of weld metal austenite content on the critical pitting temperature from the modulation of high current phase (in blau eingezeichnet die ermittelte Korrosionsbeständigkeit des Grundwerkstoffes)

As already mentioned, the corrosion resistance was higher with lower heat input (3,34 kJ/cm). The background could be the distribution and type of austenite grains, which Brytan already referred to [5]. The austenite was columnar and more homogeneously distributed in the "ferrite grain" than at higher line energy.

Further, on, it therefore seems more purposeful to qualify pulse-modulated TIG welding per se by proving that this process variant does not generally lead to a greater loss of corrosion resistance than DC processes at the material thickness investigated.

Conclusion

Pitting resistance in pulse modulated TIG welding was evaluated for single phase modulation.

i. The welds had a higher ferrite content than the base metal and had a slightly lowered pitting resistance than the base metal in the passivated state.

ii. With the modulation of the pulse phases, a comparable austenite content can be achieved as with the pure DC process.

iii. The investigations show that with a modulated high current phase at low energy per unit length the highest resistance to pitting corrosion is achieved

iv. Flank modulation yielded the highest phase fraction of austenite, but does not result in a higher critical pitting temperature.

Support

The project „PuWiDu - pulsmoduliertes WIG-Schweißen von Duplexstählen“ is supported by the Federal Ministry of Economics and Climate Protection under the funding number 49MF190173 following a resolution of the German parlament. We are grateful for this funding and support.

REFERENCES

[1] DVS MB 0946: Empfehlungen zum Schweißen von nicht rostenden austenitisch- ferritischen Duplex- und Superduplexstählen. Stand Feb/2004..

[2] Informationsstelle Edelstahl Rostfrei Merkblatt 823 „Schweißen von Edelstahl Rostfrei“, Düsseldorf 2018.

[3] Norsok Standard M601-16. Welding and inspection of piping. Lysaker, Norway: Standards Norway; 2016.

[4] Alvarez-Armas, I.; Degallaix-Moreuil, S.: Duplex Stainless Steels. Wiley, 2013 (ISTE). DOI: https://doi.org/10.1002/9781118557990

[5] Brytana, Z.; Niagajb, J.; Reimana, L.: Corrosion studies using potentiodynamic and EIS electrochemical techniques of welded lean duplex stainless steel UNS S82441. In: Applied Surface Science, Volume 388, Part A, 112/2016, pp. 160-168. DOI: https://doi.org/10.1016/j.apsusc.2016.01.260.

[6] Hertzman, S.: The Influence of Nitrogen on Microstructure and Properties of Highly Alloyed Stainless Steel. In: ISIJ International, Volume 41, Issue 6, 06/2001. pp. 580–589. DOI: https://doi.org/10.2355/isijinternational.41.580

[7] de Lima, M. S. F.; de Carvalho, S. M.; Teleginski, V.; Pariona, M.: Mechanical and Corrosion Properties of a Duplex Steel Welded using Micro-arc or Laser. In: Materials Research, Volume 18 Number 4, 08/2015 pp.723-731. DOI: http://dx.doi.org/10.1590/1516-1439.007115

[8] Karlsson, L.: Welding Duplex Stainless Steels — A Review Of Current Recommendations. In: Welding in the World Volume 56, 05/2012, pp. 65–76. DOI: https://doi.org/10.1007/BF03321351

[9] Pettersson C.-O., Holmquist M. and Mårtensson C.: Tube-to-tube sheet welding and expansion of the super duplex steel SAF 2507 (UNS S32750) at the fabrication of heat exchangers. In: Proceedings Stainless Steels ‘96, Dusseldorf/Neuss, 06/1996, pp. 184-191.

[10] Westin E.M.: Pitting corrosion resistance of GTA welded lean duplex stainless steel. Welding in the World, Volume 54, issue 11-12, 11/2010, pp. R308-321. DOI: https://doi.org/10.1007/BF03266745

[11] Chehuan, T.; Dreilich, V.; Assis, K. S. de; Sousa, F. V.V. de; Mattos, O. R: Influence of multipass pulsed gas metal arc welding on corrosion behaviour of a duplex stainless steel. Corrosion Science, Volume 86, 09/ 2014, pp. 268-274. DOI https://doi.org/10.1016/j.corsci.2014.06.004

[12] Moura, V.S.; Lima, L.D.; Pardal, J.M.; Kina, A.Y.; Corte, R.R.A.; Tavares, S.S.M.: Influence of microstructure on the corrosion resistance of the duplex stainless steel UNS S31803. Materials Characterization Volume 59, Issue 8, 08/2008, pp. 1127-1132. DOI: https://doi.org/10.1016/j.matchar.2007.09.002

[13] Yousefieh, M.; Shamanian, M.; Satchi, A.: Influence of Heat Input in Pulsed Current GTAW Process on Microstructure and Corrosion Resistance of Duplex Stainless Steel Welds. In: J Journal of Iron and Steel Research, International, Volume 18, Issue 9, 09/2011, pp. 65-69. DOI: https://doi.org/10.1016/S1006-706X(12)60036-3

[14] Pak S.; Karlsson L.: Optimizing the properties of duplex stainless weld metals by addition of nitrogen. In: Scandinavian Journal of Metallurgy, Volume 19, Issue 1, 1990, pp. 9-13.

[15] Wang, S.-H.; Chiu, P.-K.; Yang, J.-R.; Fang, J.: Gamma (γ) phase transformation in pulsed GTAW weld metal of duplex stainless steel. In: Materials Science and Engineering: A, Volume 420, Issues 1–2, 03/2006, pp. 26-33. DOI: https://doi.org/10.1016/j.msea.2006.01.028

[16] Palmer, T. A.; Elmer, J. W.: Wong, J.: In situ observations of ferrite – austenite transformations in duplex stainless steel weldments using synchrotron radiation. In: Science and Technology of Welding and Joining, Volume 7, Issue 3, 03/2002, pp. 159-171. DOI. http://dx.doi.org/10.1179/136217102225004194

[17] Yousefieh, M.; Shamanian, M.; Satchi, A.: Optimization of the pulsed current gas tungsten arc welding (PCGTAW) parameters for corrosion resistance of super duplex stainless steel (UNS S32760) welds using the Taguchi method. In: Journal of Alloys and Compounds Volume 509, 01/2011, pp. 782–788. DOI: https://doi.org/10.1016/j.jallcom.2010.09.087

[18] SchellhaseM.: Der Schweißlichtbogen – ein technologisches Werkzeug; In: DVS-Fachbuchreihe Schweißtechnik Band 84, DVS Verlag GmbH, Düsseldorf 1985, ISBN 9783871551000.

[19] Dzelnitzki, D: WIG - Gleichstromschweißen mit hochfrequenten Impulsen, eine interessante

Verfahrensvariante. In: EWM Hightec Welding GmbH, 2000.
[20] Qi, B.J.; Yang, M.; Cong, B.Q.: The effect of arc behaviour on weld geometry by high-frequency pulse GTAW with oCr18Ni9Ti stainless steel. In: The International Journal of Advanced Manufacturing Technology, Volume 66, issue 9-12, 08/2012, pp. 1545-1553. DOI: https://doi.org/10.1007/s00170-012-4438-z
[21] Yang, Z.; Mingxuan, Y.; Bojin, Q.: Fluid and arc behaviour with ultra high frequency pulsed GTAW. In: Quarterly Journal of the Japan Welding Society, Volume 33, Issue 2, 09/2015, pp. 11s-14s. DOI: https://doi.org/10.2207/qjjws.33.11s
[22] Yang, M.; Yang, Z.; Bojin, Q.: The effect of pulsed frequency on the plasma jet force with ultra high-frequency pulsed arc welding. In: Welding in the World, Volume 59, Issue 6, 11/2015. pp. 875–882. DOI: https://doi.org/10.1007/s40194-015-0261-0
[23] Knopp, N., Killing, R.: WIG-Schweißen mit Impulsen im höheren Frequenzbereich. In: EWM Hightec Welding GmbH, 2002
[24] Mehdi, B.; Badjia,R.; Jib, V.; Allilic, B.; Bradaic, D.; Deschaux-Beaumed, F.;Soulié, F.: Microstructure and residual stresses in Ti-6Al-4V alloy pulsed and unpulsed TIG welds. In: Journal of Materials Processing Technology, Volume 231, 05/2016, pp. 441-448. DOI: https://doi.org/10.1016/j.jmatprotec.2016.01.018
[25] Wang, Y.; Cong, B.; Qi, B.; Yang, M.; Lin, S.: Process characteristics and properties of AA2219 aluminum alloy welded by double pulsed VPTIG welding. In: Journal of Materials Processing Technology, Volume 266, 01/2019, pp. 255-263. DOI: https://doi.org/10.1016/j.jmatprotec.2018.11.015
[26] Wang, L. L.; Wei, H. L.; Xue, J. X.; DebRoy, T.: Special features of double pulsed gas metal arc welding. In: Journal of Materials Processing Technology, Volume 251, 01/2018, pp. 369-375. DOI: https://doi.org/10.1016/j.jmatprotec.2017.08.039
[27] Verma, J.; Taiwade, R.V.: Effect of welding processes and conditions on the microstructure, mechanical properties and corrosion resistance of duplex stainless steel weldments—A review. In: Journal of Manufacturing Processes, Volume 25, 01/2017, pp.134-152. DOI: https://doi.org/10.1016/j.jmapro.2016.11.003
[28] Tang, Y.; Dai, N.; Wu, J.; Jiang, Y.; Li, J.: Effect of Surface Roughness on Pitting Corrosion of 2205 Duplex Stainless Steel Investigated by Electrochemical Noise Measurements. In: Materials (Basel), Volume 12, Issue 5, 03/2019. DOI: : https://doi.org/10.3390/ma12050738
[29] Westin, E.M.; Hertzmann, S.: Element distribution in lean duplex stainless steel welds. In: Weld in the World Volume 58, Issue 2, 03/2014, pp. 143–160. DOI: https://doi.org/10.1007/s40194-013-0108-5,
[30] Johansson, M.M.; Westin, E. M.; Oliver, J.; Pettersson, R. F. A.: Localized Corrosion Resistance Of Welded Austenitic And Lean Duplex Stainless Steels. In: Weld in the World Volume 55, issue 9-10, 09/2011, pp. 19-27.DOI: https://doi.org/10.1007/BF03321316
[31] Liljas, M.; Gemmel, G.: Choice of specifi cations and design codes for duplex stainless steels, Proceedings Duplex America 2000, Houston, TX, Paper DA2-031, 2000, pp. 199-209.
[32] Hsieh, R.-H.; Liou, H.-Y.; Pan, Y.-T.: Effects Of cooling time and alloying elements on the microstructure of the gleeble-simulated heat-affected zone of 22% Cr Duplex stainless Steels. Journal of Materials Engineering and Performance, Volume 10, 10/2001, pp. 526–536. DOI: https://doi.org/10.1361/105994901770344665